

Scientific Journal of King Faisal University: Basic and Applied Sciences



Enhancing the Surface Properties of Additively and Conventionally Manufactured 18Ni300 Maraging Steel through Gas Nitriding

Syed Sohail and B Chandra Mohan Reddy

Department of Mechanical Engineering, JNTUA College of Engineering Ananthapuramu, Constituent college of Jawaharlal Nehru Technological University Anantapur, Ananthapuramu, India

partificiti of ivice framear En
首都

LINK	RECEIVED ACCEPTED PUBLISHED ONLI			NE ASSIGNED TO AN ISSUE		
https://doi.org/10.37575/b/eng/250030	13/08/2025	13/11/2025	13/11/2025	01/12/2025		
NO. OF WORDS	NO. OF PAGES	YEAR	VOLUME	ISSUE		
6375	7	2025	26	2		

ABSTRACT

The aim of this study was to investigate the differences in microstructure and microhardness between additively manufactured (AM) and conventionally manufactured (CM) 18Ni300 maraging steel, after subjecting samples to a low-temperature gas nitriding treatment in the solution-annealed condition. A microstructural characterization revealed equiaxed grains in CM specimens, whereas AM specimens contained irregular martensitic laths, reflecting their distinct solidification and thermal histories. Nitriding at 360° C resulted in effective case depths of approximately $60 \,\mu m$ for AM and $55 \,\mu m$ for CM specimens, values that were attributed to the enhanced nitrogen diffusivity and reduced competition with intermetallic precipitate formation at this temperature. The surface microhardness reached $1115\pm15 \,HV0.01$ for AM and $1909\pm15 \,HV0.01$ for CM, with a gradual decrease toward core hardness values of $560\pm6 \,HV0.01$ and $548\pm6 \,HV0.01$, respectively. The superior hardening response for the AM specimens is associated with their columnar grain morphology and higher dislocation density, which facilitate nitrogen trapping and strengthening. These findings demonstrate that when combined with low-temperature nitriding, additive manufacturing offers a promising method of achieving enhanced surface properties in maraging steel components intended for high-performance tool industry applications.

KEYWORDS

Metal 3D printing, microhardness, microstructure, surface engineering, strength steel, surface properties

CITATION

Syed Sohail, S. and Reddy, B.C.M. (2025). Enhancing the surface properties of additively and conventionally manufactured 18ni300 maraging steel through gas nitriding. Scientific Journal of King Faisal University: Basic and Applied Sciences, 26(2), 43—49. DOI: 10.37575/b/eng/250030

1. Introduction

Additive manufacturing (AM), commonly known as 3D printing, has revolutionized modern manufacturing by enabling the layer-by-layer fabrication of complex geometries directly from digital models (Di Angelo *et al.*, 2020). Of the various AM techniques that are available, metal additive manufacturing (MAM) has attracted significant attention for its potential to produce high-strength, functional metal parts for demanding applications in the aerospace, automotive, biomedical, and tooling industries (Herzog *et al.*, 2016). Within the field of MAM, laser powder bed fusion (LPBF) stands out as one of the most widely adopted technologies due to its ability to produce components with excellent mechanical properties, fine detail resolution, and high material utilization rates (Fayazfar *et al.*, 2018). In LPBF, a high-energy laser is employed to selectively melt and fuse metallic powders spread across a build platform, thus allowing for the creation of intricate and near-net-shape parts.

Of the various types of high-strength steels, maraging steels are notable due to their unique combination of ultra-high strength, excellent toughness, and minimal distortion during heat treatment (Hall and Slunder, 1968). The exceptional properties of these steels are achieved through a process known as age hardening, which involves the precipitation of intermetallic compounds in a low-carbon, iron-nickel matrix (Li *et al.*, 2023; Sohail and Reddy, 2025a). One of the most widely used grades within this class is 18Ni300 maraging steel (MS), which contains approximately 18% nickel with additions of cobalt, molybdenum, and titanium. This specific composition results in outstanding mechanical properties, making 18Ni300 particularly suitable for critical applications involving aerospace, tooling, and high-performance components (Guo *et al.*, 2022; Vasques *et al.*, 2025).

Several studies have investigated the influence of the LPBF process parameters on the resulting microstructure of 18Ni300 MS (Vishwakarma *et al.*, 2020; Takata *et al.*, 2018), which is generally

referred to as the as-built or as-printed microstructure. For instance, Takata et al. (2018) evaluated the as-printed microstructure of LPBF 18Ni300 MS, with a focus on the crystallographic features associated with localized melting and solidification. The presence of lath martensite inside columnar grains and retained austenite has also been reported in earlier investigations (Godec et al., 2021; Godec et al., 2022; Guo 2024). Vishwakarma et al. (2020) analyzed the influence of the build orientation on the mechanical tensile performance, and correlated the behavior with the unique microlevel grain structure. Marattukalam et al. (2020) examined the effect of scanning strategies on the resulting microstructure, texture, and mechanical properties after printing. Tan et al. (2017) thoroughly explored the evolution of the as-built microstructure, with detailed characterizations, including a study of the correlation between the typical hierarchical cellular microstructure and the corresponding mechanical properties. Solution- and aging-treated variants were also analyzed. These authors also compared the high performance obtained by AM 18Ni300 MS with that of its conventional counterpart.

Despite the ongoing research into the optimization of core properties, some recent investigations have highlighted the need to address the improvement of surface mechanical properties of LPBF 18Ni300 MS for strategic applications (Funch *et al.*, 2022; Godec *et al.*, 2021; Godec *et al.*, 2022; Sohail and Reddy, 2025b). Funch *et al.* (2022) found that simultaneous aging and gas nitriding is not a viable strategy for AM maraging steels, primarily due to the inevitable competition between precipitate and nitride formation at the (required) nominal temperatures. They also discussed the shallow case depths achieved through nitriding-aged components and highlighted the importance of prior homogenizing heat treatment to optimize the efficiency of nitriding. Hong *et al.* (2021) observed that when plasma nitriding was conducted after the aging process, this resulted in thinner nitrided layers and the lowest wear resistance relative to other nitrided variants. Their findings

indicated that the nitriding performance of solution-treated samples was markedly superior, as corroborated by both microstructural and wear analyses. Godec *et al.* (2022) examined the behavior of directly (plasma) nitrided 18Ni300 MS after LPBF processing. These authors reported that higher nitriding temperatures cause crack formation in the surface layer due to micro- and nano-level segregation, along with the formation of austenite. In another experimental study, Godec *et al.* (2021) attempted to improve the wear and corrosion resistance of selective laser-melted 18Ni300 MS. After analyzing the morphologies of plasma-nitrided specimens under various heat treatment conditions and comparing them to directly nitrided specimens, these authors proposed that the application of common heat treatments prior to nitriding is essential to achieve a crack-free compound layer.

Unlike plasma nitriding, gas nitriding is a diffusion-based treatment in which ammonia is used to infiltrate nitrogen into the heated surface. Since plasma nitriding relies on ionization in a vacuum, the low-temperature nitriding attempted in the present study would not be feasible with a plasma-based method of nitriding. Moreover, as the intended application of 18Ni300 MS (i.e. in the tool industry) involves complex geometrical features, plasma nitriding would be a poor choice compared to gas nitriding, which is preferred for the surface hardening of intricate components. This is consistent with existing studies in the literature concerning plasma nitriding of 18Ni300 MS, in which the treatment has been conducted at high temperatures in the range 440–520°C (Godec *et al.*, 2021; Godec *et al.*, 2022; Hong *et al.*, 2021).

It is clear from the above discussion that although extensive research has been conducted on optimizing the process parameters of additively manufactured 18Ni300 MS in order to enhance its core properties, along with some limited studies on high-temperature plasma nitriding of 18Ni300 MS for surface hardening, there have been very few studies that have examined the effect of low-temperature gas nitriding on AM 18Ni300 MS. Hence, this experimental study investigates the influence of a low-temperature gas nitriding heat treatment on the microstructure and microhardness of conventional and additively manufactured 18Ni300 MS specimens that have undergone a prior solution heat treatment.

2. Material and Methods

SLM specimens were printed using a dual-laser STLR-400 metal 3D printer in a nitrogen atmosphere. The 18Ni300 powder particles were examined using TESCAN Compact SEM equipment, as illustrated in Figure 1. The specimens were printed using the optimal process parameters recommended by the manufacturer, as detailed in Table 1. In addition, a stripe-pattern scanning strategy with a 67° rotational contour was employed during printing. Specimens with dimensions of $10 \times 10 \times 10$ mm were fabricated.

Figure 1. SEM images of AM 18Ni300 powder: (a) lower magnification (b) higher magnification.

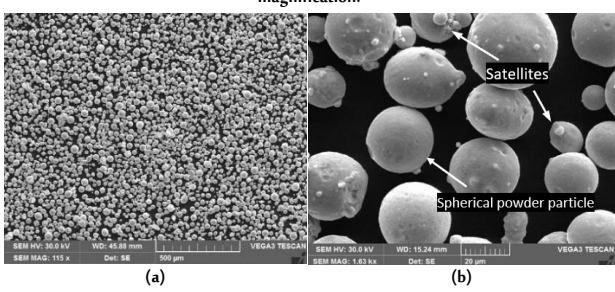


Table 1. AM process parameters

Process parameter	Magnitude		
Laser power	250W		
Scanning speed	850 mm/s		
Hatch distance	0.1mm		
Platform temperature	100°C		
Layer thickness	50 µm		

Solution treatment was performed at 900°C for 2 h in an annealing furnace under a nitrogen atmosphere, in order to homogenize the specimens completely. The samples were polished with grit sizes of up to 2000 before solution treatment. Following the method of Funch et al. (2022), nitriding was carried out at 360°C for 40 h in a pure ammonia atmosphere using a vertical gas nitriding furnace. Lowtemperature gas nitriding for extended durations effectively enhances surface nitride formation while limiting the precipitation of intermetallic compounds. This process promotes surface hardening rather than core strengthening, as in high-temperature gas nitriding. Prior to nitriding, AM and CM specimens underwent solution treatment, followed by polishing with up to 3000 grit paper, and final polishing using a 1 µm diamond suspension. As a pre-treatment, all samples were oxidized in air at 400°C for 1 h in the furnace to enhance nitrogen infiltration through surface activation. This short duration of the pre-treatment step ensures that oxides are limited to the surface, thereby maximizing the availability of nitride formers, which, in the case of 18Ni300 MS, are titanium and molybdenum. The presence of nitride formers such as these is essential for achieving optimal nitriding performance. The chemical composition of the CM and AM specimens was verified using optical emission spectroscopy and was found to be within the standard range for 18Ni300 MS (Table 2). Microstructural analysis was conducted using an Olympus BX53M optical microscope (OM) after standard metallographic preparation and etching (2% Nital, 15 s). To enable evaluation of the nitrided layer, cross-sections were etched with 5% Nital (2 min) and observed under OM. Microhardness profiles were measured with a 10 g load, a 15 s dwell time, and 10 μm spacing from the nitrided surface. For statistical purposes, three indentations were taken for each surface hardness measurement, and their average values were plotted. The as-printed AM microstructure was further analyzed via SEM using a ZEISS EVO 18 system.

Table 2. Chemical composition of AM and CM 18Ni300 MS

Element		Ni	Со	Mo	Ti	Al	C	Fe
Content	AM 18Ni300	18.28	9.25	4.94	0.121	0.121	< 0.01	Bal.
(wt.%)	CM 18Ni300	18.33	8.21	4.89	0.601	0.079	< 0.01	Bal.

3. Results and Discussion

3.1. Microstructure Profiles:

3.1.1. Microstructure in The As-Built and Annealed Conditions

The SEM micrographs in Figure 2(a) display the typical overlapping half-ellipse melt pools on the as-printed AM specimen, which form as a result of the fusion of intra-layer and inter-layer beads during the laser-based melting and solidification processes. The higher-magnification images in Figure 2(b) reveal the hierarchical cellular microstructure, which forms owing to the characteristic rapid melting and solidification during LPBF. The varying cell orientations that can be observed in Figure 2(b) are attributed to directional heat flow during layer solidification, as revealed by the angle of sectioning (Ansell *et al.*, 2020; Jagle *et al.*, 2017; Kim *et al.*, 2020; Tan *et al.*, 2017). This is partially dependent on the scanning strategy, due to its direct impact on the local heat transfer conditions at the interface between the melt pools (Jia *et al.*, 2021).

Several studies in the literature have concluded that the 67° interlayer rotational scanning used in this study causes the grain growth to be primarily elongated along the build direction, with a complex

grain structure (Taheri et al., 2023; Geiger et al., 2016; Hu et al., 2022; Marattukalam et al., 2020; Song et al., 2019; Zheng et al., 2024). The thermal heat flux between the printed layers paves the way for the formation of columnar and cellular grains, as can be seen from Figure 2(b). It is worth noting that the columnar grains branch in a direction perpendicular to that of the adjacent melt pool boundary. Moreover, cellular grains are also observed near some of the boundaries. The presence of columnar and cellular grains has been attributed to the extremely high cooling rates that occur during LPBF and the corresponding non-uniform thermal flux across the laser tracks (Bai et al., 2017; Song et al., 2019; Tan et al., 2017). This observation contrasts with the random texture commonly observed in conventionally processed specimens, which can be attributed to the thermomechanical processing steps. A more detailed discussion of these processes will be provided in subsequent sections. Complex heating and cooling dynamics have also been linked to the presence of hierarchical cellular microstructures in AM materials, which have been found to exhibit both coarse and fine grains (Vishwakarma et al., 2017). In the present study, the identified features contribute to the establishment of a microstructure characterized by a preferred orientation, which may offer significant advantages for AM specimens during thermochemical processing. Laser re-irradiation of overlapping melt pools creates coarse cells, whereas rapid cooling at the center results in fine cellular grains, similar to those in conventionally welded areas (Tan et al., 2017). This heterogenous melt pool arrangement is also attributed to the distinct nitriding performance exhibited by AM specimens, as discussed in later sections, both after solution treatment and when subjected to gas nitriding.

During the AM process of specimen printing, the lower layers experience cyclical heating and cooling, due to heat transfer from the newly added layers above. As a result, the characteristic blocks typically observed in conventional martensitic microstructures are absent from the specimens considered in this study, as revealed in Figure 2. Furthermore, the presence of heterogeneous microstructural features has the potential to enhance the formation of nitrides by accelerating nitrogen diffusion, as evidenced by findings reported in related studies (Godec *et al.*, 2021).

Figure 2. Microstructure of AM specimen in as-built condition (without annealing);
(a) low magnification; (b) high magnification.

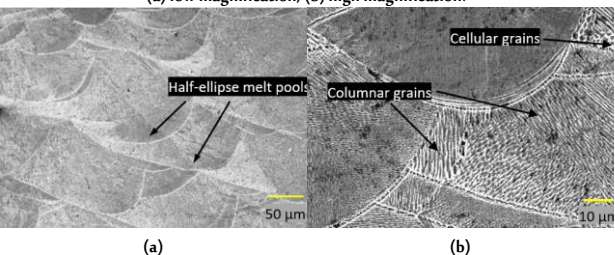
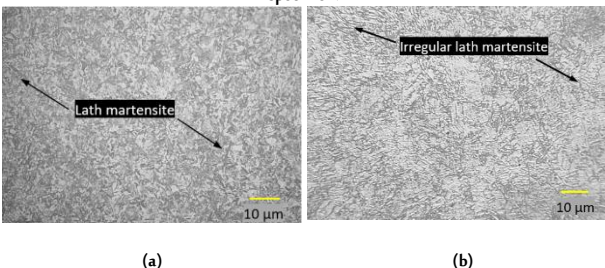


Figure 3. Microstructure in the solution-annealed condition: (a) AM specimen; (b) CM specimen.



The OM micrographs in Figure 3 show the AM and CM specimens following solution heat treatment. The laser scan tracks from the asprinted microstructure were dissolved through recrystallization.

Solution treatment not only homogenizes the microstructure but also reduces the residual stresses caused by thermal gradients during LPBF and cold working in AM and CM specimens, respectively. Furthermore, both AM and CM specimens display the characteristic lath martensite found in 18Ni300 MS (Fonseca et al. 2021). Specifically, the AM cellular structure was replaced by lath martensite, as can be observed in Figure 2. The AM specimen in the as-printed state contains retained austenite, as a result of the incomplete transformation of total austenite to martensite due to rapid solidification during laser-based AM (Ma et al., 2022). ST also has the effect of transforming the retained austenite into typical lath martensite. Although both the AM and CM specimens contain lath martensite, the AM specimen displays a slightly irregular pattern; this may result from the heterogeneous melt pool arrangement in the AM specimen, unlike the homogeneous processing of the CM specimen.

3.1.2. Microstructure in the Nitrided Condition

Gas nitriding after solution treatment has been reported to promote the smooth ingress of nitrogen onto the exposed (clean) surfaces (Funch *et al.*, 2022). Although nitrogen diffusion is temperature-dependent (i.e., higher the nitriding temperature, higher the diffusion rate), a homogenizing heat treatment such as solution treatment has been found to be imperative before gas nitriding, even for nitriding at higher temperatures (Mittemeijer *et al.*, 2015). Such treatments release any residual stresses from prior cold working operations for conventionally fabricated materials, and convert the heterogenous zones in AM materials to uniform and stress-free zones.

Figure 4. Microstructure in the nitrided condition: (a) AM specimen; (b) CM specimen.

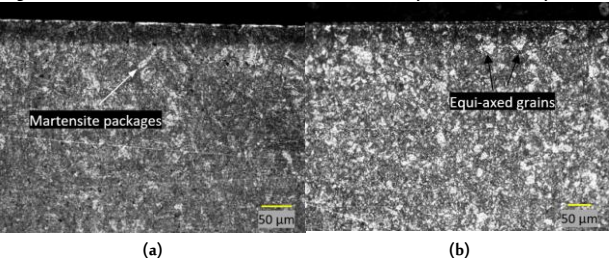
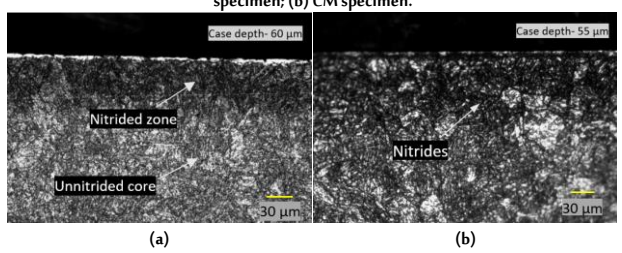


Figure 4 displays the OM microstructure of AM and CM specimens after nitriding. Etching reveals the darker nitrided zones at the top of both specimens, against the brighter un-nitrided core. The CM specimen is found to contain equiaxed grains, due to the difference in the processing route. The irregular pattern in the AM specimen that was noted after solution treatment remains after gas nitriding, as shown in Figure 4(a), with martensite laths present as packages in the grains (Godec *et al.*, 2021). Based on the OM micrographs, the nitrided AM specimen appears to have a higher nitrided depth than the CM counterpart. This is discussed in more detail in Section 3.2.

Earlier investigations have explored the effect of directly nitriding as-built AM MS. Godec *et al.* (2022) suggested a lower plasma nitriding temperature for 18Ni300 MS. At higher nitriding temperatures, cracks on the surface of the specimen were reported, which arose as a result of the characteristic residual stress zones in as-built AM components. In the current study, since the nitriding temperature was deliberately chosen with a lower magnitude and the specimen was subjected to solution annealing, cracks were not seen, as can be observed from Figs. 4(a) and (b). Moreover, although the AM specimen showed some defects in the form of spherical pores, it is important to mention that similar defects have been noted after LPBF processing of several AM metallic materials (Gong *et al.*, 2015; Hojjatzadeh *et al.*, 2020; Peng and Chen 2018), especially for 18Ni300 MS (Bai *et al.*, 2022), and are therefore typical features at some locations in AM-processed components.

The presence of these pores has a dual impact on nitriding performance, with both advantageous and disadvantageous effects. On the one hand, it promotes nitrogen infiltration, since spherical pores, especially if they are open or interconnected, provide internal surfaces and alternative short-circuit diffusion paths for nitrogen atoms to penetrate the material faster than through the bulk crystalline structure. This phenomenon may result in the development of deeper, although potentially less uniform, nitrided regions surrounding the pores in the surface of the specimen. In this study, it was noted that the nitrided zone has a nearly uniform depth, indicating that the impact of pores was relatively limited. On the other hand, the presence of numerous pores within the nitrided layer may adversely affect the overall mechanical performance of the material. This porosity reduces the effective cross-sectional area, and can consequently lead to a lower fatigue life and strength compared to a fully dense nitrided material (Sanaei and Fatemi, 2020). In addition, although nitrogen can form stable nitrides, it can also form molecular nitrogen gas (N2) within closed pores if supersaturation is reached. The high pressure of this trapped N₂ gas can plastically deform the surrounding metal matrix, and cause the pores to bulge or expand, further exacerbating the material defects. As the nitriding potential in this study was low, no such phenomenon was noted, as confirmed in Figure 5. Hence, although pores can act as diffusion facilitators, their presence can complicate the nitriding process and can compromise the integrity of the final nitrided layer, potentially negating some of the expected enhancements in the mechanical properties. Hot isostatic pressing is a common post-processing technique for AM parts, and is conducted to minimize porosity before treatments such as nitriding to ensure optimal results, as demonstrated for additively manufactured 18Ni300 MS by Song et al. (2022).

Figure 5. Microstructure in the nitrided condition, with high magnification: (a) AM specimen: (b) CM specimen.



Some researchers have made efforts to perform aging heat treatment before nitriding (Funch et al., 2022; Hong et al., 2021). Funch et al. (2022) compared the microstructure of specimens that were gas nitrided in the solution annealed condition with those in the aged condition, and observed lower nitrided case depths for agedcondition nitriding, even with variation in nitriding temperature. This was attributed to difficulties in the conversion of intermetallic precipitates (formed during prior aging) into nitrides. In this study, since nitriding was performed in the solution-annealed condition, the nitrogen uptake was anticipated to be higher, leading to the formation of nitride platelets. Figure 4(b) depicts the plate-like nitrides observed in both the AM and CM specimens. Although solution treatment before nitriding has been reported to have a limited effect on the hardness profile, the application of aging heat treatment before nitriding has been concluded in many investigations, such as those by Funch et al. (2022) and Hong et al. (2021), to be counter-productive for effective nitrogen penetration. Hong et al. (2020) concluded that the plasma nitriding performance of nitrided-aged SLM components has resulted in thinnest nitride layer compared to nitriding not-aged components, in addition it is giving the poorest tribological properties.

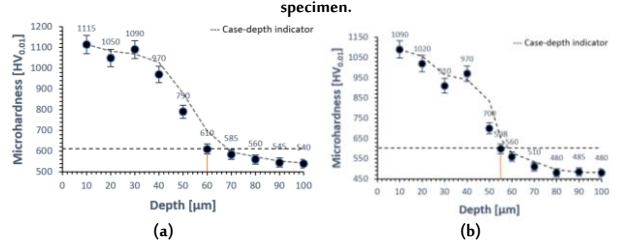
3.2. Microhardness in the Nitrided Condition:

Figure 6 illustrates the microhardness values at the nitrided surfaces of the AM and CM specimens. The microhardness values show a gradient near the surface, as a result of the higher nitride content and adsorbed interfacial nitrogen, as confirmed in earlier investigations (Funch *et al.*, 2022). The nitrogen in the alloying element nitrides is generally considered to be immobile, along with the interfacial nitrogen (Mittemeijer *et al.*, 2015). Although nitrogen is contained in these two specimens in different forms, it is unable to diffuse deeper even when further thermal processing stages are applied. The strengthening caused by the nitrogen present in the *bcc* martensite matrix and the interfacial nitrogen could also pose additional barriers to the efficient diffusion of nitrogen.

Another form of nitrogen in the thermodynamics of gas nitriding has been referred to as 'excess nitrogen' (Somers *et al.*, 1989). Due to the lower nitriding temperature used in the present study, the excess nitrogen cannot diffuse deeper to form nitrides at higher case depths. As a result, the strain induced in the *bcc* lattice could also contribute to the higher microhardness values observed near the surface of the specimen. Moreover, it is interesting to note that despite the availability of strong and intermediate nitride formers in the solutionannealed condition, such as Ti and Mo, respectively, there still seems to be insufficient nitride formation. This is evident from the absence of a rapid case-core transition in either specimen (as shown in Figure 6), a characteristic feature of strong interaction between alloying elements and nitrogen (Hosmani *et al.*, 2007).

Although the microhardness profiles of the AM and CM specimens seem to be similar, the hardness values are higher for the AM specimen, with a maximum difference of almost 12% in the microhardness values attained for the two metallurgical conditions. This finding is in line with the microstructural differences discussed in Section 3.1. The profile originating from the prior thermal history induces the formation of martensite laths in the columnar grains, as a result of the rapid solidification and melting during AM (Figure 4(a)), whereas the previously existing austenite grains dominate in the CM specimen. The small polygonal austenite grains in the CM specimen can be observed in Figure 4. The highest microhardness achieved for the nitrided AM specimen was noted as $1115 \pm 15 \, \text{HV}_{0.01}$, whereas for the nitrided CM specimen, the highest hardness was $1090 \pm 15 \, \text{HV}_{0.01}$ (at the surface in both cases).

Figure 6. Microhardness profiles in the nitrided condition: (a) AM specimen; (b) CM $\,$



The role played by the alloying elements in the nitriding behavior is also of significant interest. The elevated levels of cobalt and molybdenum present in the AM specimen, in comparison to its CM counterpart, are likely to explain its enhanced surface hardness. The observed reduction in microhardness at approximately 30 µm in both specimens suggests a deficiency of active nitride-forming alloying elements. It is worth mentioning here that studies in literature in which attempts have been made to perform nitriding and aging treatments simultaneously (at relatively high temperatures) have reported a conflict between the formation of nitrides and intermetallic precipitates, owing to the limited availability of alloying elements. The low thermal conditions employed during the gas nitriding process in this experimental study appear to

restrict the formation of the fine nitrides that are typically produced by titanium, which is recognized as a strong nitride former. Moreover, the conditions considered here were not sufficient to induce the formation of intermetallic precipitates. This conclusion is supported by a consistent decline in microhardness, which ultimately stabilized at a relatively uniform core hardness level, as illustrated in Figure 6. It is plausible that the implementation of a reduction step following the oxidation pre-treatment could enhance the nitriding kinetics by further increasing the availability of active alloying elements that form nitrides, and specifically titanium and molybdenum. This process would generate compressive residual stresses and form a denser nitride layer on the surface of the specimen, thereby improving the fatigue performance of 18Ni300 MS (Sanaei et al., 2020). Further research with sophisticated analytical techniques may yield additional insights into the specific impact of alloying elements on the nitriding behavior of MSs. The high dislocation density in AM components, particularly near the surface, contributes to its increased microhardness and facilitates the enhanced diffusion of nitrogen. This finding follows from the observations of previous investigations (Godec et al., 2021), which have concluded that although residual stresses are relieved after the post-printing heat treatment, the grain morphology arising from the typical conditions during AM affects the dislocation density, which influences the penetration of nitrogen near the surface. There was a sudden decline in microhardness after a case depth of 30 µm, for both the AM and CM specimens, up to about 60 µm. This decline was followed by a slight decrease in microhardness until the core hardness was reached (i.e., 560±6 HV_{0.01} and 548±6 HV_{0.01} for the AM and CM specimens, respectively). One possible reason for the lower core hardness in CM is the presence of a higher austenite grain morphology, even at the core microstructure level, as can be observed from the higher-magnification images in Figure 5(b). The nitrided case depth, defined as the depth at which microhardness exceeds the core value by 50 HV, was measured as approximately 60 and 50 µm for the AM and CM specimens, respectively, as depicted in Figure 6.

4. Conclusion

The present study investigated the influence of low-temperature gas nitriding on the microstructural evolution and surface characteristics of additively and conventionally manufactured 18Ni300 MS in the solution-annealed condition. Based on the observations, the main findings can be summarized as follows:

- The influence of the processing route was noted for the lowtemperature nitrided components of additively and conventionally manufactured specimens. Equi-axed grains were observed for the nitrided conventional specimen, whereas irregularly spaced martensite laths were noted for the nitrided additively manufactured specimen.
- 2. At a higher magnification, the microstructure of the nitrided additive specimen revealed the prior austenite grains in the conventional specimen; however, the additive specimen did not clearly show the presence of austenite grain boundaries. Nitride formation was noted under both metallurgical conditions, an effect that is linked to the distinct manufacturing history of the additive and conventional components.
- 3. Nitriding case depths of 60 and 55 µm were achieved through the differently nitrided route (low-temperature gas nitriding) for the additive and conventional specimens, respectively. This effect arose due to the smooth diffusion of nitrogen in the solution-annealed condition and early nitride formation, and the lower competition with the intermetallic precipitates typically observed during high-temperature nitriding.
- 4. Microhardness values as high as 1115±15 HV_{0.01} and 1090±15 HV_{0.01} were achieved at the nitrided surfaces of the additive and conventional specimens, respectively. The hardness plateau dropped suddenly between 30 and 60 µm for both metallurgical conditions, and then gradually matched the core hardness values of 560±6 HV_{0.01} and 548±6 HV_{0.01} for the additive and conventional specimens, respectively.
- 5. The additive specimen exhibited higher microhardness values

- compared to its conventional counterpart, as a result of the columnar grains in the build direction (from the prior thermal history); these influenced the dislocation density even during gas nitriding in the solution-annealed condition.
- 6. Low-temperature nitriding at 360°C could not lead to core strengthening through the significant formation of intermetallic precipitates, as is generally achieved after aging heat treatment of 18Ni300 MS. Hence, core hardness values of 560 ±6 HV_{0.01} and 548 ± 6 HV_{0.01} were attained for the additive and conventional 18Ni300 MS specimens, respectively.

The unique processing of AM parts could be leveraged to achieve deeper case depths and microhardness values through gas nitriding, which would ultimately optimize the surface properties in terms of enhanced wear, fatigue, and corrosion resistance. This emerging laser-based metal printing technology offers significant advantages for the fabrication of intricate die geometries with 18Ni300 MS.

Data Availability Statement

The data that support the findings of this study are available from the corresponding author upon reasonable request.

Acknowledgement

The authors wish to express their gratitude for support received from the funding agencies of the 'All India Council of Technical Education' for a doctoral fellowship and 'The Institution of Engineers (India)' for R and D Grant-in-Aid.

Funding

This research did not receive a specific grant from any funding agency in the public, commercial, or not-for-profit sectors.

Conflict of Interest

The authors declare no conflict of interest.

Biographies

Syed Sohail

Department of Mechanical Engineering, JNTUA College of Engineering Ananthapuramu, Constituent College of Jawaharlal Nehru Technological University Anantapur, Ananthapuramu, India, 00919032392723, syedsohail321@gmail.com.

Sohail is a Ph.D. scholar in Mechanical Engineering at JNTUA College of Engineering, Ananthapuramu. He holds an M.E. in CAD/CAM, and his research focuses on additive manufacturing, surface engineering, and maraging steels. Formerly a JRF and SRF, he has published research on machining and post-processing of 3D-printed metals. With strong academic and industrial experience in CAD/CAE and sustainable manufacturing, he actively contributes to workshops, FDPs, and collaborative projects advancing sustainable manufacturing practices.

ORCID: 0000-0003-4932-4893

B Chandra Mohan Reddy

Department of Mechanical Engineering, JNTUA College of Engineering Ananthapuramu, Constituent College of Jawaharlal Nehru Technological University Anantapur, Ananthapuramu, India, 00919490738404, cmr_b.mech@jntua.ac.in.

Prof. Reddy is a Professor of Mechanical Engineering at JNTUA College of Engineering, Ananthapuramu, with over 25 years of academic and industrial experience. He holds a Ph.D. in Mechanical Engineering and has successfully led several funded projects, including DRDO-sponsored research. His areas of expertise include advanced manufacturing, surface engineering, composite materials, thermal systems, and gas turbines. A distinguished researcher, he has authored over 50 papers in reputed journals and conferences and is a life member of ISTE and IEI.

ORCID: 0000-0002-4738-2662

References

- Andani, N.T., Safaei, K., Poorganji, B. and Elahini, M. (2023). Rotating scanning strategies for tailoring crystallographic texture of additively manufactured NiTi shape memory alloy. *Materials Letters*, 340(12), 134156. DOI: 10.1016/j.matlet.2023.134156.
- Ansell, T.Y., Ricks, J.P., Park, C., Tipper, C.S. and Luhrs, C.C. (2020). Mechanical Properties of 3D-Printed Maraging Steel Induced by Environmental Exposure. *Metals*, **10**(2), 218. DOI: 10.3390/met10020218.
- Bai, Y., Yang, Y., Wang, D. and Zhang, M. (2017). Influence mechanism of parameters process and mechanical properties evolution mechanism of maraging steel 300 by selective laser melting. *Materials Science and Engineering: A,* **703**(n/a), 116–23. DOI: 10.1016/j.msea.2017.06.033.
- Bai, Y., Zhao, C., Wang D. and Wang, H. (2022) Evolution mechanism of surface morphology and internal hole defect of 18Ni300 maraging steel fabricated by selective laser melting, *Journal of Materials Processing Technology*, 299(n/a), 117328. DOI: 10.1016/j.jmatprotec.2021.117328.
- Di Angelo, L., Di Stefano, P. and Guardiani, E. (2020). Search for the optimal build direction in additive manufacturing technologies: A review. *Journal of Manufacturing and Materials Processing,* **4**(3), 71. DOI: 10.3390/jmmp4030071.
- Fayazfar, H., Salarian, M., Rogalsky, A., Sarker, D., Russo, P., Paserin, V. and Toyserkani, E. (2018). A critical review of powder-based additive manufacturing of ferrous alloys: Process parameters, microstructure and mechanical properties. *Materials and Design*, 144(n/a), 98–128. DOI: 10.1016/j.matdes.2018.02.018.
- Fonseca, D., Feitosa, A.M., Melo, F., de Carvalho, L., Lesley, R. and Padilha, A. (2021). A short review on ultra-high-strength maraging steels and future perspectives. *Materials Research*, **24**(n/a), 20200470. DOI: 10.1590/1980-5373-MR-2020-0470.
- Funch, C.V., Christiansen, T.L. and Somers, M.A.J. (2022). Gaseous nitriding of additively manufactured maraging steel; nitriding kinetics and microstructure evolution. *Surface and Coatings Technology*, 432(n/a), 128055. DOI: 10.1016/j.surfcoat.2021.128055.
- Geiger, F., Kunze, K. and Etter, T. (2016). Tailoring the texture of IN738LC processed by selective laser melting (SLM) by specific scanning strategies. *Materials Science and Engineering: A*, 661(n/a), 240–46. DOI: 10.1016/j.msea.2016.03.036.
- Godec, M., Podgornik, B., Kocijan, A., Donik, C. and Balantic D.A.S. (2021). Use of plasma nitriding to improve the wear and corrosion resistance of 18Ni-300 maraging steel manufactured by selective laser melting. *Scientific Reports*, **11**(n/a), 3277. DOI: 10.1038/s41598-021-82572-y.
- Godec, M., Ruiz-Zepeda, F., Podgornik, B., Donik, C., Kocijan, A. and Skobir Balantic, D.A. (2022). The influence of the plasma nitriding temperature on the microstructure evolution and surface properties of additive-manufactured 18Ni300 maraging steel. Surface and Coatings Technology, 433(n/a), 128089. DOI: 10.1016/j.surfcoat.2022.128089.
- Gong, H., Rafi, K., Gu, H., Ram, J., Starr, T. and Stucker, B. (2015). Influence of defects on mechanical properties of Ti-6Al-4V components produced by selective laser melting and electron beam melting. *Materials and Design*, **86**(n/a), 545-54. DOI: 10.1016/j.matdes.2015.07.147.
- Guo, L. (2024). Characterization of Microstructure and High Strain Rate Deformation Response of C250 Maraging Steel Fabricated by Directed Energy Deposition Process. PhD Thesis, University of Manitoba, Canada.
- Guo, L., Zhang, L., Andersson, J. and Ojo, O. (2022). Additive manufacturing of 18% nickel maraging steels: Defect, structure and mechanical properties: A review, *Journal of Materials Science and Technology*, 120(n/a), 227–52. DOI: 10.1016/j.jmst.2021.10.056.
- Hall, A. and Slunder, C. (1968). *The Metallurgy, Behavior, and Application of the 18-Percent Nickel Maraging Steels, 20000828 057, NASA 36.*Available at: https://apps.dtic.mil/sti/tr/pdf/ADA382105.pdf.
- Herzog, D., Seyda, V., Wycisk, E. and Emmelmann, C. (2016). Additive manufacturing of metals. *Acta Materialia*, **117**(n/a), 371–92. DOI: 10.1016/j.actamat.2016.07.019.
- Hojjatzadeh, S.M.H., Parab, N.D., Guo, Q., Zhao, C., Qu, M., Escano, L.I., Fezzaa, K., Sun, T. and Chen, L. (2020). Direct observation of pore formation mechanisms during LPBF additive manufacturing process and high energy density laser welding. *International Journal of Machine Tools and Manufacture*, **153**(n/a), 103555. DOI: 10.1016/j.ijmachtools.2020.103555.

- Hong, Y., Dong, D.D., Lin, S.S., Wang, W., Cai, X.Y. and Zhuang, L.Z. (2021). Improving surface mechanical properties of the selective laser melted 18Ni300 maraging steel via plasma nitriding. *Surface and Coatings Technology*, 406(n/a), 126675. DOI: 10.1016/j.surfcoat.2020.126675\.
- Hosmani, S.S., Schacherl, R.E. and Mittemeijer, E.J. (2007). Kinetics of nitriding Fe-2 Wt Pct V alloy: Mobile and immobile excess nitrogen. *Metallurgical and Materials Transactions A*, **38**(n/a), 7–16. DOI: 10.1007/s11661-006-9046-9.
- Hu, Z., Yang, Z., Du, Z., Wu, J., Dong, J., Wang, H. and Ma, Z., (2022). Effect of scanning strategy on the anisotropy in microstructure and properties of Cu-Cr-Zr alloy manufactured by laser powder bed fusion. *Journal of Alloys and Compounds*, 920(n/a), 165957. DOI: 10.1016/j.jallcom.2022.165957.
- Jagle, E.A., Sheng, Z., Kurnsteiner, P., Ocylok, S., Weisheit, A. and Raabe, D. (2017). Comparison of maraging steel micro- and nanostructure produced conventionally and by laser additive manufacturing. *Materials*, 10(1), 8. DOI: 10.3390/ma10010008.
- Jia, H., Sun, H., and Wang, H., Wu, Y. and Wang, H. (2021). Scanning strategy in selective laser melting (SLM): A review, *The International Journal of Advanced Manufacturing Technology*, **113**(n/a), 2413–35. DOI: 10.1007/s00170-021-06810-3.
- Kim, D., Kim, T., Ha, K., Oak, J., Jeon, J.B., Park, Y. and Lee, W. (2020). Effect of Heat Treatment Condition on Microstructural and Mechanical Anisotropies of Selective Laser Melted Maraging 18Ni-300 Steel. Metals, 10(3), 410. DOI: 10.3390/met10030410.
- Li, K., Yang, T., Gong, N., Wu, J., Wu, X., Zhang D.Z. and Murr, L.E. (2023).

 Additive manufacturing of ultra-high strength steels: A review.

 Journal of Alloys and Compounds, 965(n/a), 171390. DOI: 10.1016/j.jallcom.2023.171390.
- Ma, Y., Gao, Y., Zhao, L., Li, D. and Men, Z. (2022). Optimization of process parameters and analysis of microstructure and properties of 18Ni300 by selective laser melting. *Materials*, **15**(n/a), 4757. DOI: 10.3390/ma15144757.
- Marattukalam, J.J., Karlsson, D., Pacheco, V., Beran, P., Wiklund, U., Jansson, U., Hjorvarsson, B. and Sahlberg, M., (2020). The effect of laser scanning strategies on texture, mechanical properties, and site-specific grain orientation in selective laser melted 316L SS. *Materials and Design*, **193**(n/a), 108852. DOI: 10.1016/j.matdes.2020.108852.
- Mittemeijer, E.J. and Somers, M.A. (2015). *Thermochemical surface engineering of steels*. Woodhead Publishing, Cambridge.
- Peng, T. and Chen, C. (2018). Influence of energy density on energy demand and porosity of 316L stainless steel fabricated by selective laser melting. *International Journal of Precision Engineering and Manufacturing- Green Technology*, 5(n/a), 55–62. DOI: 10.1007/s40684-018-0006-9.
- Sanaei, N. and Fatemi, A. (2020). Defects in additive manufactured metals and their effect on fatigue performance: A state-of-the-art review, *Progress in Materials Science*, **117**(n/a), 100724. DOI: 10.1016/j.pmatsci.2020.100724.
- Sohail, S. and Reddy, B.C.M. (2025a). Experimental investigation on end milling behavior of additively and conventionally manufactured 18Ni300 maraging steel, proceedings of the international conference on advanced materials, manufacturing and sustainable development (ICAMMSD 2024). *Atlantis Press*, n/a(n/a), 525–42. DOI: 10.2991/978-94-6463-662-8_42.
- Sohail, S. and Reddy, B.C.M. (2025b). Optimizing surface roughness in end milling of additively and conventionally manufactured components of 18Ni300 maraging steel with minimum quantity lubrication. *Engineering Research Express*, 7(1), 015503. DOI: 10.1088/2631-8695/ada22e.
- Somers, M.A.J., Lankreijer, R.M. and Mittemeijer, E.J. (1989). Excess nitrogen in the ferrite matrix of nitrided binary iron-based alloys. *Philosophical Magazine A*, 59(2), 353–78. DOI: 10.1080/01418618908205064.
- Song, J., Tang, Q., Chen, H., Zhang, Z., Feng, Q., Zhao, M., Ma, S. and Setchi, R. (2022). Laser powder bed fusion of high-strength maraging steel with concurrently enhanced strength and ductility after heat treatments. *Materials Science and Engineering: A*, **854**(n/a), 143818. DOI: 10.1016/j.msea.2022.143818.
- Song, J., Tang, Q., Feng, Q., Ma, S., Setchi, R., Liu, Y., Han, Q., Fan, X. and Zhang, M. (2019). Effect of heat treatment on microstructure and mechanical behaviours of 18Ni-300 maraging steel manufactured by selective laser melting. *Optics and Laser Technology*, **120**(n/a), 105725. DOI: 10.1016/j.optlastec.2019.105725.

- Takata, N., Nishida, R., Suzuki, A., Kobashi, M. and Kato, M. (2018). Crystallographic features of microstructure in maraging steel fabricated by selective laser melting. *Metals*, 8(6), 440. DOI: 10.3390/met8060440.
- Tan, C., Zhou, K., Ma, W., Zhang, P., Liu, M. and Kuang, T. (2017). Microstructural evolution, nanoprecipitation behavior and mechanical properties of selective laser melted high-performance grade 300 maraging steel. *Materials and Design*, **134**(n/a), 23–34. DOI: 10.1016/j.matdes.2017.08.026.
- Vasques, C.M.A., Cavadas, A.M.S. and Abrantes, J.C.C. (2025). Technology overview and investigation of the quality of a 3D-printed maraging steel demonstration part. *Materials Science in Additive Manufacturing*, 4(2), 025040002. DOI: 10.36922/MSAM025040002.
- Vishwakarma, J., Chattopadhyay, K. and Santhi Srinivas, N.C. (2020). Effect of build orientation on microstructure and tensile behavior of selectively laser melted M300 maraging steel. *Materials Science and Engineering: A,* **798**(n/a), 140130, DOI: 10.1016/j.msea.2020.140130.
- Zheng, Z., Sun, B. and Mao, L. (2024). Effect of scanning strategy on the manufacturing quality and performance of printed 316l stainless steel using SLM process. *Materials*, **17**(5), 1189. DOI: 10.3390/ma17051189.

Copyright

Copyright: © 2025 by Author(s) is licensed under CC BY 4.0. This article is an open-access article distributed under the terms and conditions of the Creative Commons Attribution (CC BY) license (https://creativecommons.org/licenses/by/4.0/).